

Quasi-Phase-Matching Efficiency Optimization for Coupled Second-Order Nonlinear Processes

Cheng-Wei Hsu¹, Jui-Yu Lai, and Shang-Da Yang²

Abstract—It is well known how to tailor the conversion efficiency grid of a single quasi-phase-matching (QPM) grating when the involved processes are uncoupled. However, it becomes much more sophisticated in the presence of coupling between multiple processes. In this case, different processes compete for the same QPM “resources” throughout the grating, and one process can outweigh the others over a certain range of interaction. Here we propose the generalized iterative domino (GID) algorithm to meet these challenges for the first time (to our best knowledge). Instead of tailoring the strength of each “global” Fourier coefficient, GID algorithm can properly adjust the spatially varying “local” Fourier coefficients in favor of the final yield. Three methods, including cascaded single-period (C1P) structure, quasi-periodic optical superlattice (QPOS), and hyperfine aperiodic optical superlattice (HAOS) optimized by GID, are numerically and experimentally investigated under the platform of third-harmonic generation (THG). It shows that the THG efficiency of HAOS + GID can exceed the record achieved by C1P structure by 33%. This method is applicable to general wavelength converters involving with multiple coupled nonlinear processes.

Index Terms—Optical wavelength conversion, optical harmonic generation, optimization methods, nonlinear optical device.

I. INTRODUCTION

QUASI-PHASE-MATCHING (QPM) outperforms birefringence phase-matching in terms of the ability of accessing the largest nonlinear tensor component, free of spatial walk-off (and beam distortion), and the flexibility of tailoring the phase-matching response by domain engineering. Pioneering works on domain engineering, such as Fibonacci optical superlattice (FOS) [1], phase reversal sequence (PRS) [2], have succeeded in converting multiple wavelengths (one at a time) in a single QPM grating. However, the reciprocal vectors (Fourier coefficients) $G(\Delta k_i)$, ($i \in \text{integer}$) that can be achieved by these early methods are far from flexible. For example, the attainable wavevector mismatch values Δk_i in FOS are subject to selection rules, while PRS can only produce uniformly spaced vectors in the reciprocal space. Although upgraded FOS eventually

enables quasi-periodic optical superlattice (QPOS) to generate arbitrary set of Δk_i [3]–[5], none of them can systematically adjust the relative strength of the Fourier coefficient $|G(\Delta k_i)|$. This weakness is solved by a series of newer methods, such as aperiodic optical superlattice optimized by simulated annealing [6], iterative optimization of grating modulation function based on superposition of cosine functions [7], nonperiodic optical superlattice optimized by genetic algorithm [8], and hyperfine aperiodic optical superlattice (HAOS) optimized by iterative domino algorithm [9]. Although full control of position and relative strength of $G(\Delta k_i)$ enabled by these methods seems sufficient to realize any multi-wavelength converter in a single QPM grating, things become more complicated when some of the interacting waves involve with more than one nonlinear process simultaneously. For example, the QPM grating in a self-doubling optical parametric oscillator (OPO) has to phase match the $\chi^{(2)}$ processes of OPO and second-harmonic generation (SHG), where the signal wave of OPO serves as the pump wave of SHG [7]. Similarly, the two pump waves of sum frequency generation (SFG) come from the fundamental and second-harmonic (SH) waves of SHG in a frequency tripler [3]–[5], [10], [11]. The coupling between nonlinear processes causes different phase-matching components are preferred at different positions in the QPM grating. In the case of frequency tripling, for example, a higher third-harmonic (TH) yield would arise if SFG starts to be phase matched after non-negligible presence of SH signal. This is taken into account in the cascaded single-period (C1P) structure made by two periodic QPM gratings dedicated to SHG and SFG in tandem [12], where the two processes are spatially decoupled. Although C1P structure has been demonstrated in a couple of occasions [12], [13], no effort has been made to optimize the section length ratio, and higher order QPM is usually needed (if some first order QPM period is too short to be fabricated) at the cost of reduced efficiency [12], [13]. An even fundamental weakness of C1P structure is the extra restriction of spatial multiplexing of different phase-matching components, which tends to degrade the conversion efficiency. In spite of these disadvantages, the THG efficiencies of aperiodic QPM gratings reported to date are still lower than that of C1P structure [3]–[5], [10], [11]. This is attributed to the fact that the existing methods only count on the “global” Fourier coefficients $G(\Delta k_i)$ (calculated by integration over the entire QPM grating), therefore, cannot realize gradual transition of “local” Fourier coefficients $G_i(x)$ (calculated by integration over a finite window) that is vital for optimizing the conversion efficiency.

Manuscript received May 23, 2019; revised August 3, 2019; accepted September 17, 2019. Date of publication September 25, 2019; date of current version November 12, 2019. This work was supported in part by the Ministry of Science and Technology (MOST), Taiwan, under Grant 104-2112-M-007-012-MY3 and Grant 107-2112-M-007-006. (Corresponding author: Cheng-Wei Hsu.)

C.-W. Hsu and S.-D. Yang are with the Institute of Photonics Technologies, National Tsing Hua University, Hsinchu 30013, Taiwan (e-mail: cw_hsu@gapp.nthu.edu.tw; shangda@ee.nthu.edu.tw).

J.-Y. Lai is with the Research and Development Department, HC Photonics Corporation, Hsinchu 30078, Taiwan (e-mail: ryan_lai@hcphotonics.com).

Color versions of one or more of the figures in this letter are available online at <http://ieeexplore.ieee.org>.

Digital Object Identifier 10.1109/LPT.2019.2943745

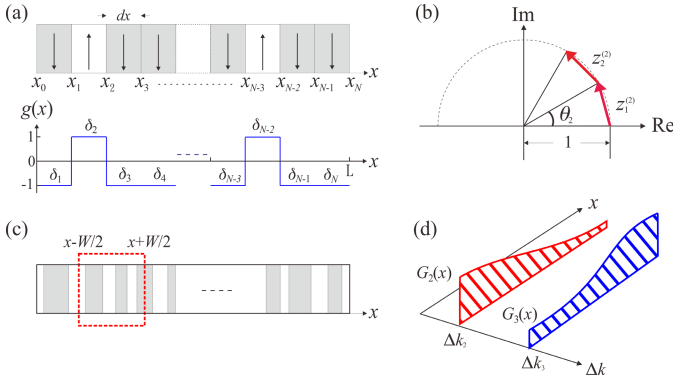


Fig. 1. (a) Schematic diagrams of HAOS and the corresponding grating modulation function. (b) Graphical representation of $z_n^{(2)}$. (c) An observation window used in calculating local Fourier coefficients. (d) Local Fourier coefficient functions $G_i(x)$ of SHG ($i = 2$) and SFG ($i = 3$).

We previously demonstrated a novel approach, HAOS optimized by iterative domino algorithm, to accomplish uncoupled multi-wavelength SHG with unprecedented conversion efficiency and computation speed [9]. In this letter, we upgrade the iterative domino algorithm by considering “local” Fourier coefficients in the presence of coupling between SHG and SFG. Numerical analysis and proof-of-concept experiments in single-wavelength THG show that the conversion efficiency achieved by our HAOS optimized by generalized iterative domino (GID) algorithm outperforms that of QPOS by ~ 4 times. A more symbolic milestone is that it exceeds the conversion efficiency “limit” of C1P structure by 33% for the first time. The ability to manipulate local Fourier coefficients of aperiodic QPM gratings makes GID algorithm highly attractive for general coupled nonlinear processes.

II. WORKING PRINCIPLE

As shown in Fig. 1(a), HAOS is composed of N unit blocks of length dx , whose orientations are specified by a piecewise binary grating modulation function $g(x)$. Under the assumptions of plane waves and constant fundamental field E_1 (non-depleted pump), the SH field at position x is formulated as

$$E_2(x) = -j\kappa_2 E_1^2 \int_0^x g(\xi) \times e^{j\Delta k_2 \xi} d\xi, \quad (1)$$

where $\Delta k_2 = k_{2\omega} - 2k_\omega$ and κ_2 denote the wavevector mismatch and coupling coefficient of the SHG process, respectively. Equation (1) means the SH field arising from an infinitesimal range of $(\xi, \xi + d\xi)$ is proportional to a complex factor $g(\xi) \times e^{j\Delta k_2 \xi} d\xi$. Given $g(x) = \{\pm 1\}$ in each unit block, the SH field at the exit of the m th unit block ($x = x_m$) can be evaluated by a 1D series

$$E_2(x_m) = -\frac{\kappa_2 E_1^2}{\Delta k_2} \sum_{n=1}^m \delta_n \times z_n^{(2)}, \quad (2)$$

where the product of $\delta_n = \{\pm 1\}$ and $z_n^{(2)} = e^{j\Delta k_2 x_n} - e^{j\Delta k_2 x_{n-1}}$ represents the coherent contribution factor of the n th unit block. Conceptually, $z_n^{(2)}$ can be illustrated as a peripheral

vector of a unit circle on the complex plane spanning over a constant angle of $\theta_2 = \Delta k_2 \times dx$ [Fig. 1(b)]. Different unit blocks correspond to vectors of the same length but different orientations.

On the other hand, the output TH field can be formulated as

$$E_3 = -j\kappa_3 E_1 \int_0^L g(x) \times e^{j\Delta k_3 x} \times E_2(x) dx, \quad (3)$$

where $\Delta k_3 = k_{3\omega} - k_{2\omega} - k_\omega$ and κ_3 indicate the wavevector mismatch and coupling coefficient of the SFG process, respectively. Substituting Eq. (1) into Eq. (3) and performing the double integral under a piecewise binary $g(x)$ result in a 2D series

$$E_3 = \frac{\kappa_3 \kappa_2}{\Delta k_2 \Delta k_3} E_1^3 \sum_{m=1}^N \left[\delta_m \times z_m^{(3)} \times \left(\sum_{n=1}^m \delta_n \times z_n^{(2)} \right) \right], \quad (4)$$

where the product of $\delta_m = \{\pm 1\}$ and $z_m^{(3)} = e^{j\Delta k_3 x_m} - e^{j\Delta k_3 x_{m-1}}$ represents the coherent contribution factor of the m th unit block in the SFG process. Since $\delta_n \times z_n^{(2)}$ and $\delta_m \times z_m^{(3)}$ tend to change abruptly from block to block, it is more informative to evaluate the normalized coherent contribution factor of blocks around position x over an observation window of length W [Fig. 1(c)]

$$G_i(x) = \frac{1}{W} \int_{x-W/2}^{x+W/2} g(\xi) \times e^{j\Delta k_i \xi} d\xi \quad (i = 2, 3). \quad (5)$$

Note that Eq. (5) reduces to $G(\Delta k_i)$, i.e. the “global” Fourier coefficient of $g(x)$ at Δk_i , if the observation window extends to the entire QPM grating. This is what the existing algorithms, including the original iterative domino algorithm, can optimize systematically. By comparison, $G_i(x)$ refers to the “local” Fourier coefficient function at the reciprocal Δk_i within $(x-W/2, x+W/2)$, providing spatial resolution for G_i .

Inspired by the iterative domino algorithm developed for optimizing uncoupled nonlinear processes, the GID algorithm handles coupled nonlinear processes by testing the block orientations one by one. If the q th block is inverted ($\delta_q \rightarrow -\delta_q$), the output TH field E_3 can be updated by manipulating two 1D series without carrying out the cumbersome 2D series of Eq. (4)

$$E_3' = E_3 - 2z_q^{(3)} \sum_{n=1}^{q-1} \delta_n \times z_n^{(2)} - 2z_q^{(2)} \sum_{n=q+1}^N \delta_n \times z_n^{(3)}. \quad (6)$$

The block inversion is preserved (or abandoned) if $|E_3'| > |E_3|$ (or $|E_3'| < |E_3|$). In each iteration, all the blocks are sequentially tested ($q = 1 \sim N$). The iteration continues until none of the N blocks needs to be inverted anymore.

III. SIMULATION

We numerically investigate THG in C1P structure, QPOS, and HAOS + GID, respectively. All of them are designed by assuming 10-mm-long 5 mol.% MgO-doped congruent lithium niobate (MgO-CLN) pumped by monochromatic plane wave of 10 kW/cm² intensity at 1560 nm wavelength. In this case, the wavevector mismatch values for SHG and SFG are $\Delta k_2 = 0.3208 \mu\text{m}^{-1}$ and $\Delta k_3 = 0.8847 \mu\text{m}^{-1}$, respectively.

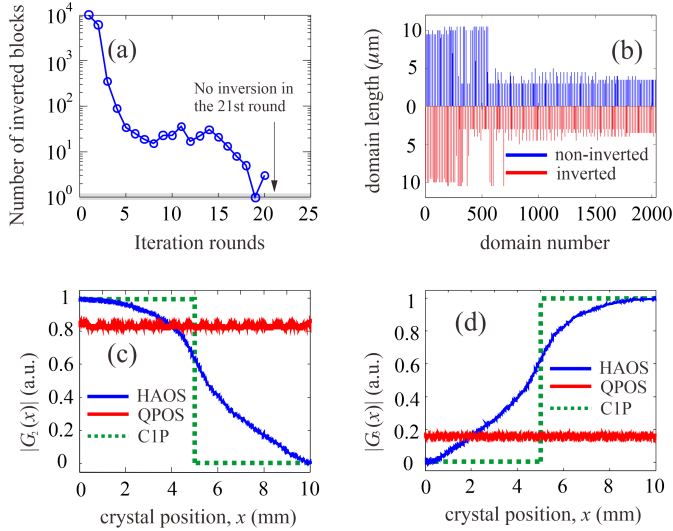


Fig. 2. (a) Evolution of the number of inverted blocks during the GID optimization. (b) Domain length distribution with the domain number in the crystal of non-inverted domain (blue) and inverted domain (red), respectively. (c, d) Local Fourier coefficient magnitude functions of HAOS (blue solid), QPOS (red solid) and CIP structure (green dotted) for (b) SHG, and (c) SFG processes, respectively.

QPOS is designed to maximize the two “global” Fourier coefficient magnitudes $|G(\Delta k_2)|$ and $|G(\Delta k_3)|$ under the parameters of $\theta = 1.2613$ rad (projection angle), $l_a^+ = l_b^+ = 10$ μm , $l_a^- = 5.1$ μm , $l_b^- = 11$ μm [5], [11]. On the other hand, 20,000 blocks, each is of 500-nm length, are used in the design of HAOS ($N = 20,000$, $d_x = 500$ nm, $L = 10$ mm). Figure 2(a) shows the evolution of the number of inverted blocks during the optimization process. It drops rapidly in the first few iterations, and converges in just 21 iterations (taking ~ 40 s). Figure 2(b) illustrates the lengths of all 2036 domains after optimization, where the decreasing trend indicates the weighting of QPM gradually transfers from SHG to SFG longitudinally.

Figures 2(c) and 2(d) show $|G_2(x)|$ and $|G_3(x)|$, the local Fourier coefficient magnitude functions (under $W = 500$ μm) of SHG and SFG, of the three approaches. The features of $|G_i(x)|$ provide an insight into the spatial dependence of TH yields (calculated by solving coupled wave equations) in different QPM gratings. As shown in Fig. 3, both HAOS (blue solid) and QPOS (red solid) produce TH yield since the crystal entrance ($x = 0$), while it only builds up in the second half of the CIP structure (green dotted). This is qualitatively consistent with the spatial distributions of $|G_3(x)|$ in Fig. 2(d), which exhibit monotonically increasing (HAOS), uniform (QPOS), and stepwise (CIP) features, respectively. Quantitatively, the THG efficiencies of HAOS, QPOS, and CIP scale as 1.33:0.32:1 (inset of Fig. 3). This result can be justified by the guideline of maximizing THG efficiency, i.e. making $|G_3(x)|$ large only in the presence of non-negligible SH signal. For example, QPOS is less efficient for it delivers the same $|G_3(x)|$ even when the SH field remains negligible. CIP structure takes the guideline into account by contributing to SFG during the second half of the crystal ($L/2 < x < L$) where the SH field has emerged noticeably. In this way,

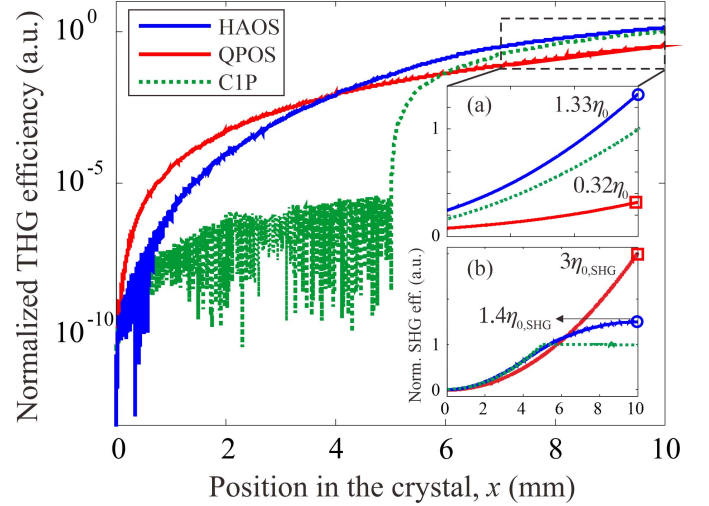


Fig. 3. Simulated spatial evolution of THG conversion efficiencies (in log scale) of HAOS (blue solid), QPOS (red solid) and first-order CIP structure (green dotted). Each curve is normalized to the final THG efficiency η_0 of CIP structure. The inset (a) (in linear scale) shows the evolution during the last 3 mm of the crystal, and (b) shows the spatial evolution of SH powers normalized to that obtained in CIP structure ($\eta_{0,SHG}$) in the three devices, respectively.

the larger Fourier coefficient magnitude of CIP outperforms the longer interaction length of QPOS and other existing aperiodic QPM grating design methods [6]–[9]. The potential of spatially varying $G_i(x)$ is truly unleashed in HAOS, where the optimized $G_3(x)$ increases with the SH field coherently. As a result, the TH yield of HAOS grows still faster than that of CIP structure in the second half of the device, and the final THG efficiency is 1.33 times larger than that of first-order CIP structure. To the best of our knowledge, this is the first time that the THG conversion efficiency of first-order CIP structure is outperformed.

IV. EXPERIMENT RESULT

We fabricate 10-mm-long MgO-CLN chips by standard mask-patterned electric poling technique to implement first-order CIP structure, QPOS and HAOS. In view of the smallest domain in aperiodic QPM gratings that can be reliably poled on a 0.5-mm-thick MgO-CLN wafer, we force the minimum domain size of HAOS as 3 μm by imposing a test-and-correction round after the end of GID optimization [9]. This technical limitation of minimum domain length reduces the theoretical THG efficiency of HAOS from 1.33 η_0 to 1.13 η_0 , where η_0 denotes the theoretical THG efficiency of first-order CIP structure. A wavelength-tunable CW laser (eTL-2100, EZconn Corp.) and an Er-doped fiber amplifier (SDO Communications Corp.) are employed to characterize aperiodic QPM gratings. The focused laser beam inside the chips is ~ 250 mW in power and 50 μm in diameter. The generated SH signal is directly measured by a silicon photodetector and a lock-in amplifier, while the TH signal is measured by the same detector placed after three dichroic filters (R $\sim 99\%$ at 780 nm). In view of the refractive index variation of MgO-CLN wafers, fundamental

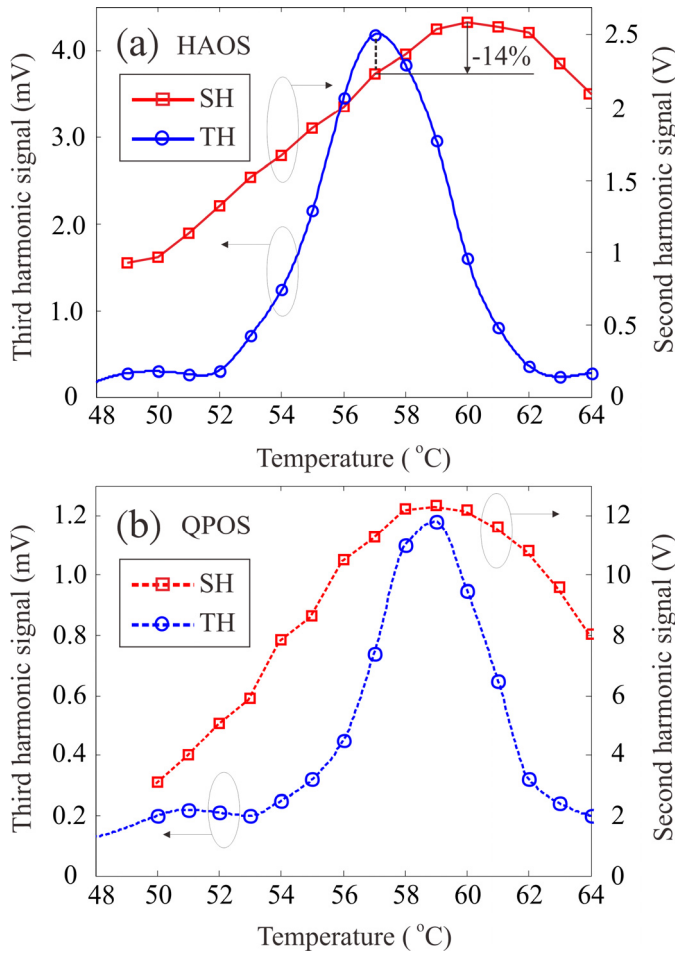


Fig. 4. Experimentally measured SH (squares) and TH (circles) signals against temperature of (a) HAOS, and (b) QPOS chips.

wavelength was set at 1560.2 nm (HAOS and C1P chips) and 1562.3 nm (QPOS chip) to maximize the TH yields. The tuning curves of SHG and SFG (Fig. 4) are characterized by tuning the temperature from 50°C to 62°C with an increment of 1°C. The experimentally measured THG efficiencies of HAOS and QPOS are $\eta_{HAOS} = 0.94\eta_{C1P}$ (at 57°C) and $\eta_{QPOS} = 0.25\eta_{C1P}$ (at 59°C) respectively. The measured ratio of η_{HAOS}/η_{C1P} is smaller than the theoretical prediction of 1.13, which is mainly attributed to the misaligned phase-matching temperatures [Fig. 4(a)] caused by the uncertainty of MgO-CLN dispersion. Note that the measured η_{C1P} is free of this issue because we used a fan-out C1P grating that can always locate a pair of periods to perfectly phase match SHG and SFG. By taking the 14% efficiency reduction into account [Fig. 4(a)], we expect to get $\eta_{HAOS}/\eta_{C1P} = 1.09$, which is very close the theoretical value of 1.13.

V. CONCLUSION

In conclusion, the GID algorithm is developed to optimize the THG efficiency of aperiodic QPM gratings. The algorithm

takes coupled $\chi^{(2)}$ processes into account, therefore, can adjust “local” Fourier coefficient functions in coherence with the spatial evolution of interacting waves. Simulation shows that HAOS optimized by GID does outperform the benchmark approaches of QPOS and C1P, where the THG efficiency exceeds the “limit” of C1P structure by 33% for the first time. In the proof-of-concept experiment, dispersion variation of MgO-CLN wafers causes misalignment between the phase-matching temperatures of SHG and SFG in the HAOS chip. By calibrating the corresponding efficiency degradation, the THG efficiency of HAOS presumably outperforms first-order C1P structure and QPOS by factors of 1.09 and 4.36, close to the theoretical predictions of 1.13 and 4.16. This innovative method is applicable to general wavelength converters involving with coupled nonlinear processes.

REFERENCES

- [1] S.-N. Zhu, Y.-Y. Zhu, Y.-Q. Qin, H.-F. Wang, C.-Z. Ge, and N.-B. Ming, “Experimental realization of second harmonic generation in a fibonacci optical superlattice of LiTaO₃,” *Phys. Rev. Lett.*, vol. 78, pp. 2752–2755, Apr. 1997.
- [2] M. H. Chou, K. R. Parameswaran, M. M. Fejer, and I. Brener, “Multiple channel wavelength conversion using engineered quasi-phase matching structures in LiNbO₃ waveguides,” in *Proc. Conf. Lasers Electro-Opt.*, May 1999, p. 219.
- [3] K. Fradkin-Kashi and A. Arie, “Multiple-wavelength quasi-phase-matched nonlinear interactions,” *IEEE J. Quantum. Elect.*, vol. 35, no. 11, pp. 1649–1656, Nov. 1999.
- [4] K. Fradkin-Kashi, A. Arie, P. Urenski, and G. Rosenman, “Multiple nonlinear optical interactions with arbitrary wave vector differences,” *Phys. Rev. Lett.*, vol. 88, Dec. 2001, Art. no. 023903.
- [5] C. Zhang, H. Wei, Y.-Y. Zhu, H.-T. Wang, S.-N. Zhu, and N.-B. Ming, “Third-harmonic generation in a general two-component quasi-periodic optical superlattice,” *Opt. Lett.*, vol. 26, no. 12, pp. 899–901, 2001.
- [6] Y. W. Lee, F. C. Fan, Y. C. Huang, B. Y. Gu, B. Z. Dong, and M. H. Chou, “Nonlinear multiwavelength conversion based on an aperiodic optical superlattice in lithium niobate,” *Opt. Lett.*, vol. 27, no. 24, pp. 2191–2193, 2002.
- [7] T. Kartaloğlu, Z. G. Figen, and O. Aytür, “Simultaneous phase matching of optical parametric oscillation and second-harmonic generation in aperiodically poled lithium niobate,” *J. Opt. Soc. Amer. B, Opt. Phys.*, vol. 20, no. 2, pp. 343–350, 2003.
- [8] J.-Y. Lai, Y.-J. Liu, H.-Y. Wu, Y.-H. Chen, and S.-D. Yang, “Engineered multiwavelength conversion using nonperiodic optical superlattice optimized by genetic algorithm,” *Opt. Express*, vol. 18, no. 5, pp. 5328–5337, 2010.
- [9] J.-Y. Lai, C.-W. Hsu, N. Hsu, Y. H. Chen, and S.-D. Yang, “Hyperfine aperiodic optical superlattice optimized by iterative domino algorithm for phase-matching engineering,” *Opt. Lett.*, vol. 37, no. 7, pp. 1184–1186, 2012.
- [10] Z. W. Liu *et al.*, “Quasi-Cw ultraviolet generation in a dual-periodic LiTaO₃ superlattice by frequency tripling,” *Jpn. J. Appl. Phys.*, vol. 40, no. 12, pp. 6841–6844, Dec. 2001.
- [11] S.-N. Zhu, Y.-Y. Zhu, and N.-B. Ming, “Quasi-phase-matched third-harmonic generation in a quasi-periodic optical superlattice,” *Science*, vol. 278, pp. 843–846, Oct. 1997.
- [12] K. Kintaka, M. Fujimura, T. Suhara, and H. Nishihara, “Third harmonic generation of Nd:YAG laser light in periodically poled LiNbO₃ waveguide,” *Electron. Lett.*, vol. 33, no. 17, pp. 1459–1461, Aug. 1997.
- [13] W.-C. Hsu, Y.-Y. Lai, C.-J. Lai, L.-H. Peng, C.-L. Pan, and A. H. Kung, “Generation of multi-octave-spanning laser harmonics by cascaded quasi-phase matching in a monolithic ferroelectric crystal,” *Opt. Lett.*, vol. 34, no. 22, pp. 3496–3498, 2009.